Journal of Nanobiotechnology

RESEARCH

Open Access

Albumin-seeking near-infrared-II probe evaluating blood–brain barrier disruption in stroke

Hong-Jing Zhu[1†], Ying-Ying Sun[1†], Yijing Du[3,4], Sheng-Yu Zhou[1], Yang Qu[1], Shu-Yan Pang[1], Shoujun Zhu[3,4*], Yi Yang[1*] and Zhen-Ni Guo[1,2*]

Abstract

Background Blood-brain barrier (BBB) disruption after stroke is closely associated with brain tissue edema and neuronal injury, which requires accurate assessment. However, there is a lack of appropriate BBB imaging modality in vivo. As albumin in the blood could cross the damaged BBB into brain tissue after stroke, it serves as a biomarker for BBB disruption. Therefore, we aimed to develop an albumin-seeking near-infrared (NIR) probe to assess BBB disruption in stroke.

Results We proposed a chemoselective strategy for seeking albumin with NIR dyes and identified an optimal probe to evaluate BBB disruption in stroke. The probe combined a NIR fluorescent dye with inherent albumin-targeting moieties and exhibited high affinity and selectivity for binding to albumin. Using a mouse stroke model, the probe displayed a high-resolution visualization of the location and extent of BBB disruption in vivo and correlated well with BBB leakage measured by Evans blue ex vivo. A dual-channel NIR-II imaging was successfully used to simultaneously assess BBB disruption and cerebral perfusion after stroke. Furthermore, we applied this method to dynamically evaluate the BBB disruption process and reperfusion of thrombolytic therapy in a stroke model in real time, which showed excellent application value.

Conclusions We developed an albumin-seeking NIR probe that accurately evaluated BBB disruption in a safe, non-invasive and real-time manner in various stroke models, and has a great potential guiding stroke treatment in a real-time manner.

[†]Hong-Jing Zhu and Ying-Ying Sun contributed equally to this work.

*Correspondence:
Shoujun Zhu
sjzhu@jlu.edu.cn
Yi Yang
yang_yi@jlu.edu.cn
Zhen-Ni Guo
zhen1ni2@jlu.edu.cn

Full list of author information is available at the end of the article

Graphical Abstract

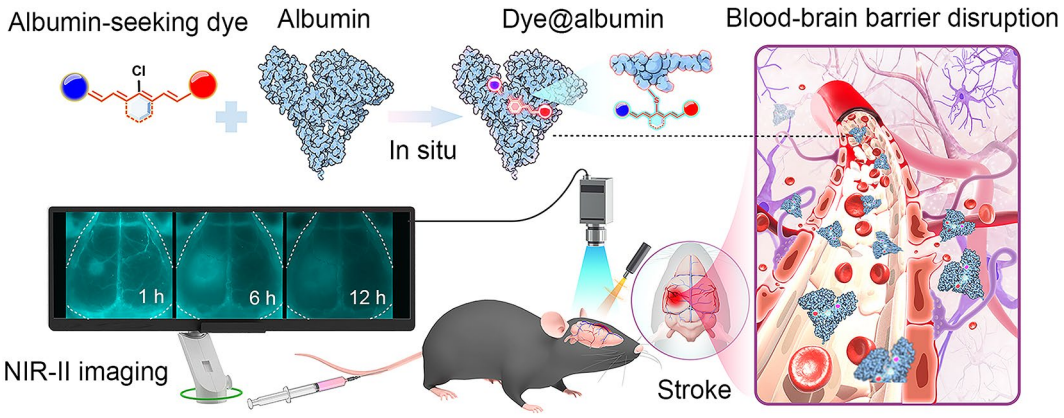

Keywords Albumin-seeking dye, Blood–brain barrier disruption, Stroke, Albumin tagging, NIR-II bioimaging

Background

Stroke is one of the leading causes of death worldwide [1], which is a severe neurological disorder involving the disruption of the blood-brain barrier (BBB) [2]. The BBB is a biological barrier composed of brain endothelial cells and tight junction proteins that restrict the entry of most substances from the bloodstream into brain tissue [3, 4]. Stroke-related inflammatory reactions and vascular injuries cause BBB disruption, resulting in brain tissue edema and neuronal damage [5, 6]. Therefore, accurate assessment of the location and extent of BBB disruption in real time is crucial for the diagnosis and treatment of stroke. However, current BBB imaging techniques, mainly including MRI, CT and two-photon microscopy [7–9], are limited for in vivo BBB assessment due to time-consuming, radiation risk or invasive restrictions [10, 11].

Near-infrared (NIR) imaging has emerged as a powerful technique for non-invasive imaging in biomedical research and clinical applications [12]. Recently, the second near-infrared window (NIR-II) has gained significant attention with low tissue autofluorescence, great tissue penetration and reduced scattering [13, 14], and making it able to provide high spatial resolution imaging at deeper tissue depths in real-time manner [15, 16]. Meanwhile, the development of NIR-II imaging probes, such as NIR-II fluorescent dyes and nanoparticles, has further enhanced the capabilities of NIR-II imaging [17–20]. The combination of NIR-II imaging and targeted probes holds great promise for a wide range of applications [21–24]. However, the development of NIR fluorescent probes specifically targeting BBB disruption in stroke remains a challenge.

As albumin in the blood crosses the damaged BBB into brain tissue after stroke, it serves as a biomarker for BBB disruption [25, 26]. According to this pathophysiological characterization, we developed an albumin-seeking NIR probe aiming to achieve high-sensitivity and high-resolution imaging of BBB disruption. The probe combines a near-infrared fluorescent dye with albumin-targeting moieties to in situ bind to albumin in the blood, and the dye-tagged albumin thus achieved specific detection of BBB disruption. The albumin-seeking dye allows for safe and accurate assessment of the extent of BBB disruption in real time in a mouse stroke model. Using NIR-II dual-channel imaging, we achieved simultaneous imaging of BBB and cerebral perfusion after stroke and applied for real-time assessment of reperfusion and BBB disruption process in thrombolytic therapy stroke model. Our study provides targeted imaging for BBB, which offers a powerful tool for studying the pathogenesis of stroke, developing novel therapeutic approaches, and evaluating treatment strategies.

Results

Albumin-seeking NIR dyes covalently combine with albumin and increase brightness

We proposed a chemoselective albumin-seeking strategy for NIR dyes binding to albumin in vivo. Previous studies have proved the covalent bonding between chlorine-containing (Cl-containing) cyanine dyes and albumin [27]. IR-780, IR-808 and IR-783 were cyanine dyes possessing chlorocyclohexene that could first enter the albumin pocket through supramolecular interactions and underwent covalent binding via a nucleophilic substitution reaction between the -SH group in albumin and the Cl-C bond in these dyes [27, 28]. While the Cl-free dye (ICG) bound albumin only through non-covalent supramolecular interactions [29]. Covalent binding of Cl-containing cyanine dyes and bovine serum albumin (BSA) enhances the stability and brightness of free cyanine dyes (Fig. 1a) [13, 30, 31]. We selected the Cl-containing NIR cyanine dyes that can covalently bind to albumin with optimal albumin-binding abilities of IR-780 > IR-808 > IR-783, and ICG as a comparison which not covalently bind to

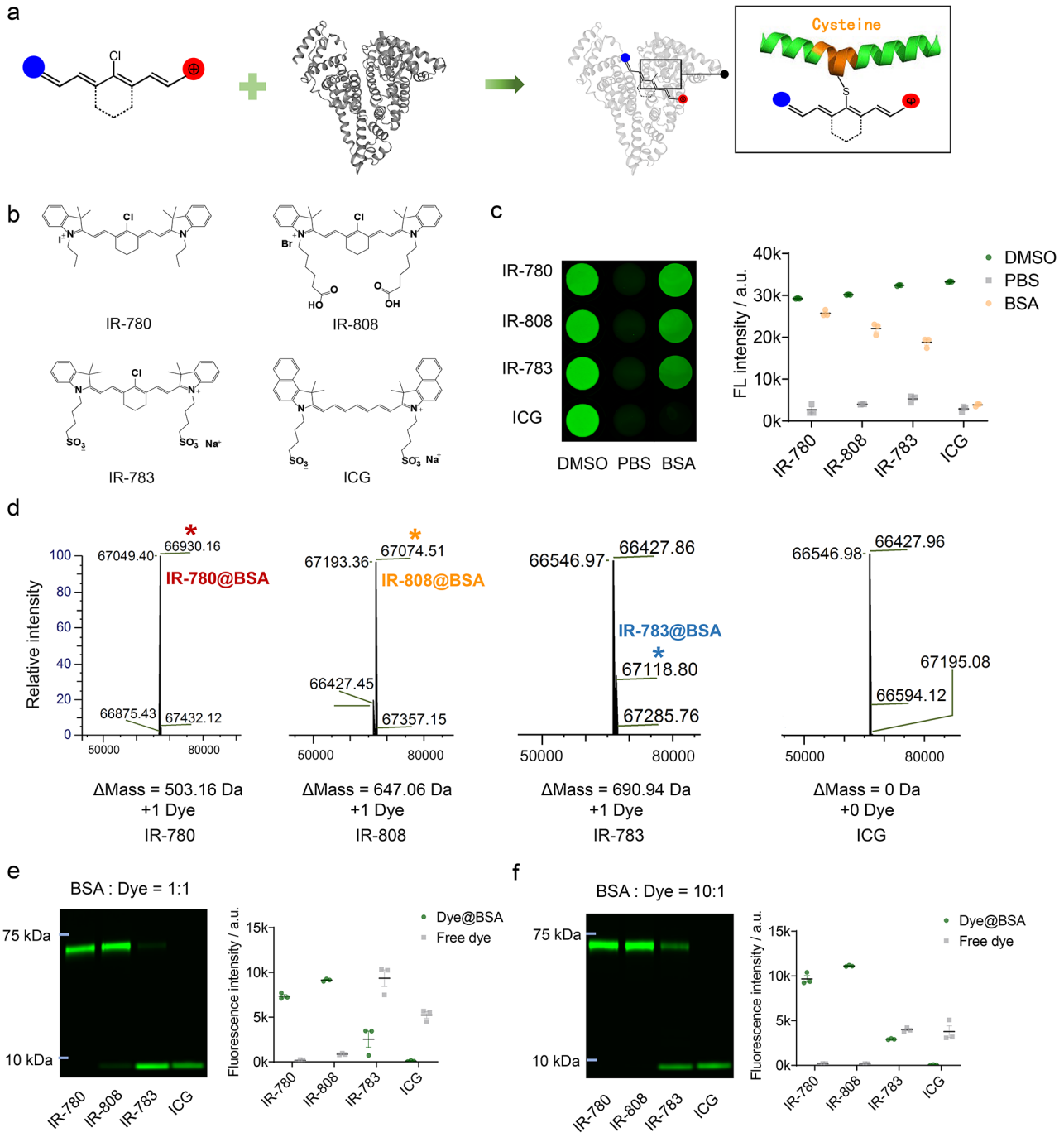

Fig. 1 Chlorine-containing albumin-seeking dyes covalently bind to albumin and increase brightness. (**a**) Schematic diagram of the covalent binding site of chlorine-containing cyanine dye and albumin. (**b**) Structural formula of IR-780, IR-808, IR-783, and ICG. (**c**) Brightness of four dyes (50 nM) in DMSO, PBS, and BSA with incubating at 60 ºC of 1:1 molar ratio (mean ± SEM, $n = 3$). (**d**) Mass spectrometric analysis of four dyes in BSA with 1:1 reaction molar ratio at 37 ºC for 2 h. (**e**-**f**) Gel electrophoretic analysis of fluorescence intensity of four dyes in BSA at 1:1 and 10:1 reaction molar ratio at 37 ºC for 2 h (mean ± SEM, $n = 3$)

albumin (Fig. 1b) [27]. First, we compared the brightness characteristics of the four probes in vitro binding to albumin. The dyes exhibited the highest and lowest brightness in DMSO and PBS, respectively. Dyes in BSA were incubated at a 1:1 molar ratio at 60 °C for 2 h. The absorption and fluorescence spectra showed that the free dyes and Dye@BSA in PBS exhibited absorption peaks at 779–799 nm with NIR-II tail emission (Fig. S1). IR-780, IR-808, and IR-783 were associated with a higher brightness forming Dye@BSA than free dyes in

PBS (Fig. 1c). In addition, compared with dyes in PBS, Dye@BSA has higher NIR-II quantum yield (Fig. S2, S3, Table S1). Next, the binding proportions of the four dyes to BSA were analyzed. Mass spectrometry illustrated that IR-780, IR-808, IR-783 bound to BSA in a 1:1 ratio (Fig. 1d). The bio-layer interferometry (BLI) experiments quantitatively compared binding affinity of IR-780 (K_D = 2.80E+04 nM) > IR-808 (K_D = 9.50E+04 nM) > IR-783 (K_D = 4.30E+05 nM) > ICG (K_D =8.10E+05 nM) (Fig. S4, Table S2). Gel electrophoresis showed that IR-780 bound almost completely to BSA, IR-808 bound mostly to BSA with a small fraction of free IR-808, IR-783 bound only partially to BSA, and ICG did not form any stable complex with BSA (Fig. 1e). As albumin is the most abundant protein in the blood, and previous studies have shown that increasing the BSA: dye ratio enhances the binding proportion [27, 32, 33]. Therefore, we further incubated BSA with dyes at a ratio of 10:1. The gel electrophoresis revealed an enhanced binding of Cl-containing cyanine dyes to BSA, with IR-780 and IR-808 binding almost completely to BSA and IR-783 exhibiting an increased binding to BSA, whereas ICG binding proportion remained unchanged (Fig. 1f).

Albumin-seeking dyes highly affinity and selectively bind to albumin in situ with enhanced brightness and circulation time

Before applying albumin-seeking dyes to stroke imaging, we observed the systemic metabolism and circulation of the four dyes in mice. After intravenous injection, IR-780 and IR-808 accumulated in the liver and then distributed throughout the whole body maintaining high brightness for approximately 72 h with a long metabolism time. In contrast, IR-783 and ICG accumulated in the liver and cleared rapidly from the body within 24 h (Fig. S5).

To verify the metabolism of dyes in the circulation and the formation of dye@albumin complexes in vivo, blood samples were collected from mice intravenously injected with the same dose of the four dyes. The serum was separated and subjected to gel electrophoresis, followed by NIR fluorescence imaging and gel staining with Coomassie Brilliant Blue. IR-780 and IR-808 maintained higher brightness in the circulation for a longer period compared to IR-783 and ICG, which gradually decreased within 7 days after the tail venous injection of the probes (Fig. 2a, b). In contrast to the results of brightness in vitro binding to albumin, IR-808 exhibited the highest brightness in circulation, followed by IR-780. It may be attributed to the hydrophobicity of IR-780, resulting in self-assembly and lower brightness when injected into the mice than IR-808 [34]. The serum gel electrophoresis results showed that IR-780, IR-808, and IR-783 formed dye@albumin complexes of approximately 66 kDa in situ, whereas ICG remained in its free form and was rapidly metabolized (Fig. 2c). Figure 2d shows the band patterns of various proteins in the serum collected at different time points. These results indicated the high selectivity and stability of IR-780, IR-808, and IR-783 binding to albumin. Consistent with the serum fluorescence brightness results, the IR-808@albumin band was the brightest and the IR-780@albumin band was the second brightest. Only a portion of IR-783 formed complexes with albumin in the bloodstream, whereas the unbound portion of the dye was quickly metabolized and excreted. ICG did not bind to endogenous albumin and exhibited the fastest metabolism, reaching its highest brightness after 1 min, which decreased rapidly 10 min post-administration (Fig. 2e). These results illustrate that albumin-seeking probes can selectively and stably bind albumin in vivo with increasing brightness and circulation time.

Albumin-seeking dyes monitoring BBB disruption in stroke mice in real-time

Albumin is normally scarce in the brain tissue. However, blood albumin enters the brain through the damaged BBB post-stroke [35, 36]. Therefore, the albumin in brain serves as a biomarker for BBB injury [25, 26]. Although the dye-albumin complex enhanced the brightness and circulation time of free dye, introducing exogenous albumin may trigger immune or inflammatory reactions [37]. Therefore, the probe that can bind to endogenous albumin in situ may offer safe imaging and good capabilities for monitoring BBB disruption.

We explored albumin-seeking dyes for visualization of BBB disruption after stroke in a photothrombotic stroke (PTS) model with infarcts in the left cerebral cortex of mice. At 30 min post stroke, IR-780, IR-808, IR-783, and ICG were intravenously injected at the same dose respectively, and real-time dynamic NIR-II imaging was performed without the need for craniotomy (Fig. 3a). As shown in Fig. 3b, cerebral vessels were visualized but no fluorophore leakage into the stroke region at 1 min after probes injection. Fluorescence signals gradually accumulated in the stroke area in the IR-780 and IR-808 groups with leakage observed as early as 10 min, indicating the accumulation in the brain parenchyma through the damaged BBB. IR-808 exhibited a brighter imaging than IR-780, consistent with the relative brightness of the serum. IR-783 have weaker brightness than IR-780 and IR-808, and showed a low fluorescence signal at 1 min. Due to the relatively weak binding affinity of IR-783 with albumin, free IR-783 cleared rapidly from the body [27]. Therefore, unbound IR-783 was rapidly metabolized and thus showed lower fluorescence signals in cerebral vascular at 10 min / 30 min / 1 h than those at 1 min. After a long period of injection into the blood circulation, IR-783 could bind to albumin and greatly enhance its fluorescence intensity, thus showing a higher fluorescence signal

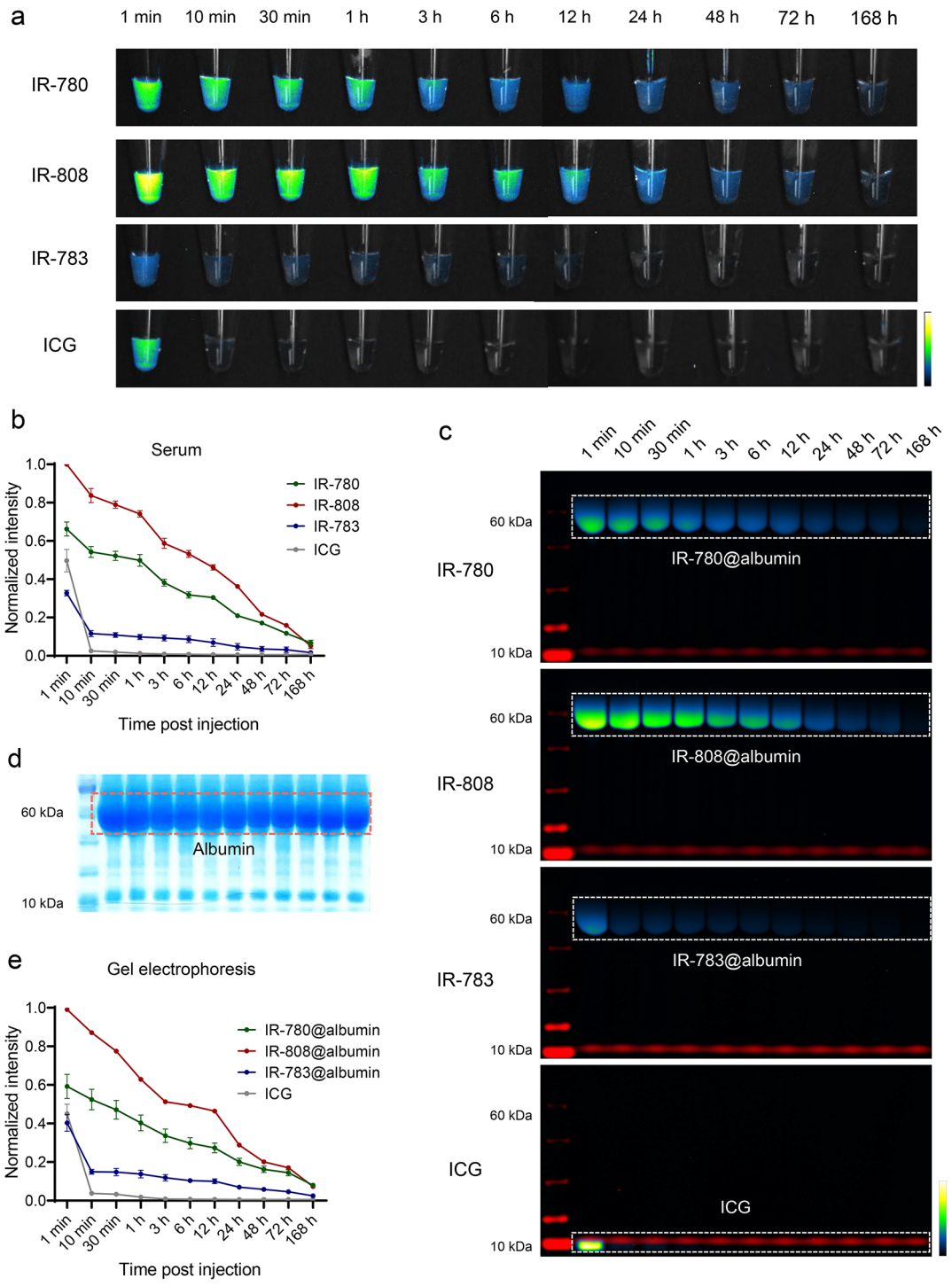

Fig. 2 Comparison of circulation metabolic behavior of albumin-seeking dyes in vivo. (**a**) Serum was collected at time points after tail vein injection (50 μM, 60 μL) of IR-780, IR-808, IR-783 and ICG and imaged under the NIR-II window (80 ms, 1100 LP). (**b**) Normalized fluorescence intensity of serum after injection of dyes (mean ± SEM, $n = 3$ for each group). (**c**) Gel electrophoresis analysis of dyes and albumin binding changed over time in mice serum. (**d**) Coomassie brilliant blue showed protein distribution of serum after gel electrophoresis. (**e**) Normalized fluorescence intensity of albumin complex band of IR-780@albumin, IR-808@albumin, and IR-783@albumin and free ICG (mean ± SEM, $n = 3$ for each group)

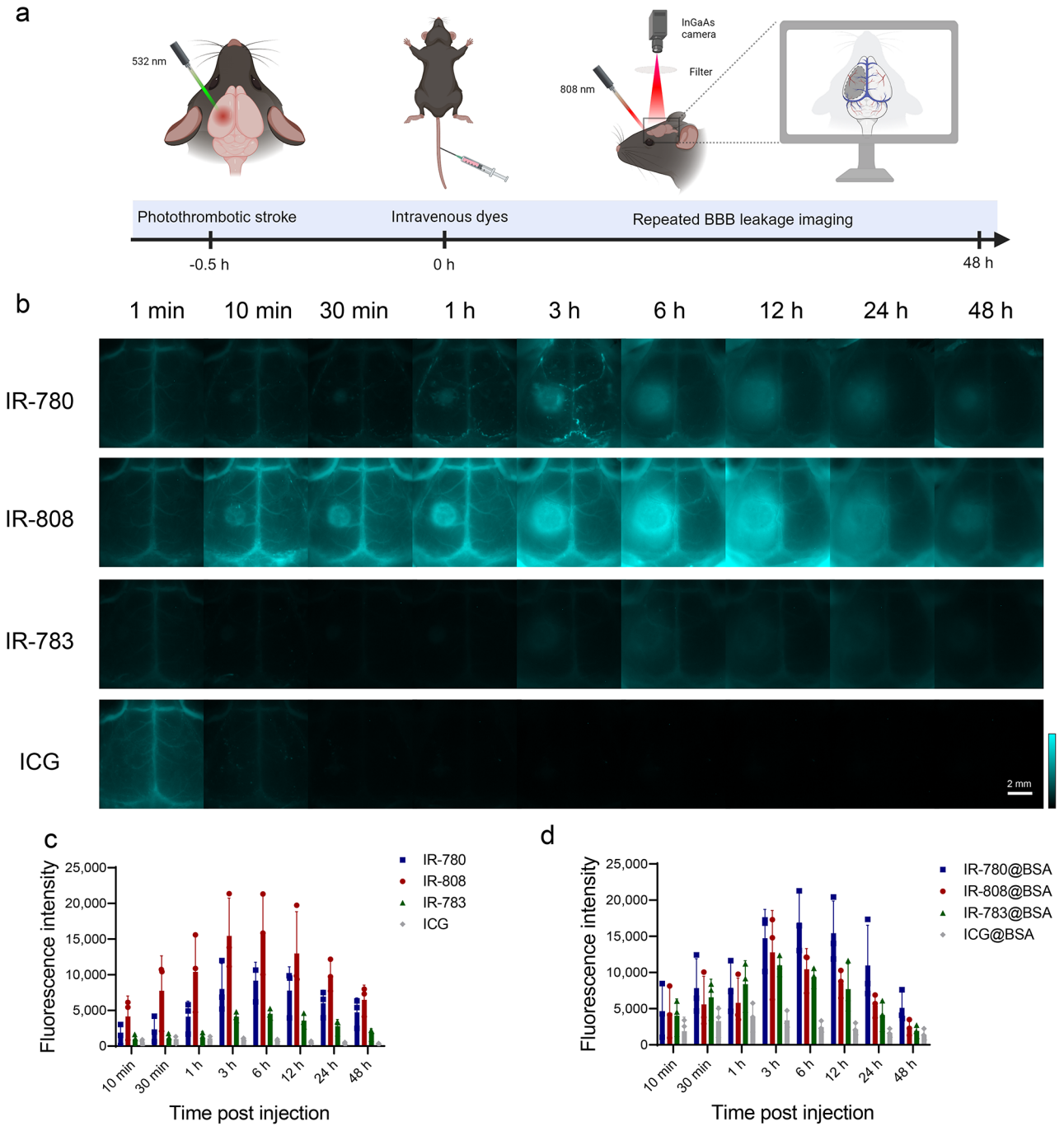

Fig. 3 Albumin-seeking dyes real-time monitoring BBB disruption in mice with stroke. (**a**) Schematic diagram of photothrombotic stroke model and NIR-II imaging for BBB disruption monitoring post-stroke (Created with BioRender.com). (**b**) NIR-II dynamic imaging (40 ms, 1100 LP) recorded at indicated time points post-injection of stroke mice with IR-780, IR-808, IR-783, and ICG (50 μM, 60 μL). (**c**-**d**) Difference in fluorescence signal intensity on the left and right sides post-injection of free dyes and dye@BSA (mean ± SEM, $n = 3$ for each group)

at 3 h than that at 10 min / 30 min / 1 h and accumulation of fluorescence signals in the BBB leakage region was observed but with lower brightness than IR-780 and IR-808. ICG showed higher brightness in the blood vessels 1 min after injection but was rapidly metabolized within 10 min, with minimal signal accumulation in the stroke area. To minimize the influence of brightness in the blood vessels, we quantified the fluorescence signal in the BBB disruption area by calculating the difference between the signal in the BBB disruption area and corresponding signal in the healthy contralateral area (Fig. 3c). IR-780, IR-808, and IR-783 showed the largest

difference in the accumulation of fluorescence signals at 6 h, whereas ICG exhibited minimal signal accumulation in the brain tissue, which gradually decreased after peaking at 1 h.

In addition, we validated the imaging ability of the BBB using the dye@BSA complex synthesized in vitro (Fig. S6a). IR-780@BSA, IR-808@BSA, and IR-783@BSA complexes exhibited similar brightness and circulation times in monitoring BBB disruption. ICG@BSA exhibited a behavior similar to free ICG. The brightness of the BBB disruption area was observed to be IR-780@BSA > IR-808@BSA > IR-783@BSA (Fig. 3d). Although IR-780 demonstrated the strongest binding ability to albumin in vitro, it did not achieve similar effects as IR-780@BSA complex in vivo, possibly because of its hydrophobicity leading to self-assembly, and insufficient binding in vivo [38]. In contrast, IR-808 has similar effects as the IR-808@BSA complex, indicating that IR-808 can serve as an ideal albumin-seeking probe for monitoring BBB disruption after stroke without the need for exogenous albumin, thus offering better biocompatibility. To confirm that BBB imaging using IR-808 relies on its in vivo binding to albumin, we used an albumin-escaping probe, IR-808AC [39], which clearly visualized blood vessels but did not accumulate nor show BBB disruption and was completely metabolized from the blood vessels within 10 min (Fig. S6b).

The albumin-seeking dyes allows for immediate assessment, multi-timepoint monitoring after stroke and a real-time, high-resolution visualization of BBB disruption. Among the four dyes tested, IR-808 exhibited the most remarkable visualization of BBB disruption. Therefore, IR-808 is a promising probe for accurate assessment of stroke injury and we conducted detailed imaging using IR-808 in our subsequent investigations.

IR-808 enables evaluation of BBB injury in strokes with various severities

We first displayed the imaging of IR-808 monitoring BBB leakage in NIR sub-windows. Fig. S7a presents the imaging results of IR-808 in NIR-I window (850–900 nm) and three sub-NIR-II windows (>1100 nm, > 1200 nm, and >1300 nm). IR-808 could provide sufficient brightness under the longer NIR-II sub-window by increasing the exposure time and improves signal-to-background ratio (SBR) compared with in NIR-I window (Fig. S7b). We next observed changes in cerebral perfusion and IR-808 fluorescence signal accumulation in acute-phase of stroke. Dynamic continuous imaging of cerebral arteries and veins in the mice was observed 2.8 s post IR-808 injection. Compared with healthy side, a reduction in cerebral perfusion was observed in the infarct area of stroke mice (Fig. S8a, b). Leakage of fluorescent signal was observed in the stroke area 5 min after injection of IR-808, and fluorescent signal accumulation increased within 1 h (Fig. S8c, d).

We further explored the efficiency of IR-808 to detect and distinguish BBB injury of sham mice and three severity levels of stroke. As described in the methods, the severity of stroke injury was graded into three groups using the PTS model [40]. TTC results showed a progressive increasing infarct volume at 24 h after stroke in mild, moderate and severe stroke groups (Fig. 4a). Western blotting analysis of protein expression in brain tissue showed a gradual decrease in tight junction-related proteins (ZO-1, occludin) and basement membrane-related protein (laminin) and an increase in matrix metalloproteinase (MMP-9) levels in the sham, mild, moderate, and severe stroke groups (Fig. 4b), indicating an increased degree of BBB disruption. NIR-II imaging shows the fluorescence signals were similar in both sides and did not leak through the intact BBB in the sham group. In stroke groups, fluorophores leakage initially in the infarct core and gradually accumulates in the peri-infarct tissue as stroke time progressing, indicating dynamic aggregation through leakage BBB into brain tissue (Fig. 4c). Relative fluorescence intensity of the affected side increased progressively after stroke. In the moderate to severe stroke, the relative fluorescence intensity peaked at 12 h, whereas in the mild stroke it increased until the 24-h peak (Fig. 4d). The BBB leakage area increased over time in stroke groups and was larger in the worse stroke groups (Fig. 4e). In addition, we analyzed statistical differences in BBB disruption between stroke severity at time points. The relative fluorescence intensity was significantly higher in the more severity stroke groups at 6 h ($P<0.01$) and 12 h ($P<0.05$) (Fig. S9a). The BBB damage area was significantly different at 6 h between the three stroke groups ($P<0.01$) and was significantly lower in mild stroke than in moderate-to-severe strokes at 12 h ($P<0.01$) (Fig. S9b). At 24 h, relative fluorescence intensity and damage area were significantly higher in severe stroke than mild stroke ($P<0.05$). These results indicate that IR-808 allows dynamic assessment of strokes, as well as good differences in leakage area and relative fluorescence intensity measured by IR-808 in various severity strokes.

BBB disruption evaluated by IR-808 correlates well with Evans blue measurement

Currently, BBB disruption in experimental animals is mainly assessed through intravenous injection of Evans blue (EB), followed by ex vivo imaging and quantification [41]. To verify the reliability of the IR-808 in vivo evaluation of BBB injury, we performed in terms of both IR-808 NIR-II imaging in vivo and EB ex vivo measurement and quantification in sections at 6 h, 12 h, and 24 h, respectively. IR-808 leakage area and fluorescence intensity as

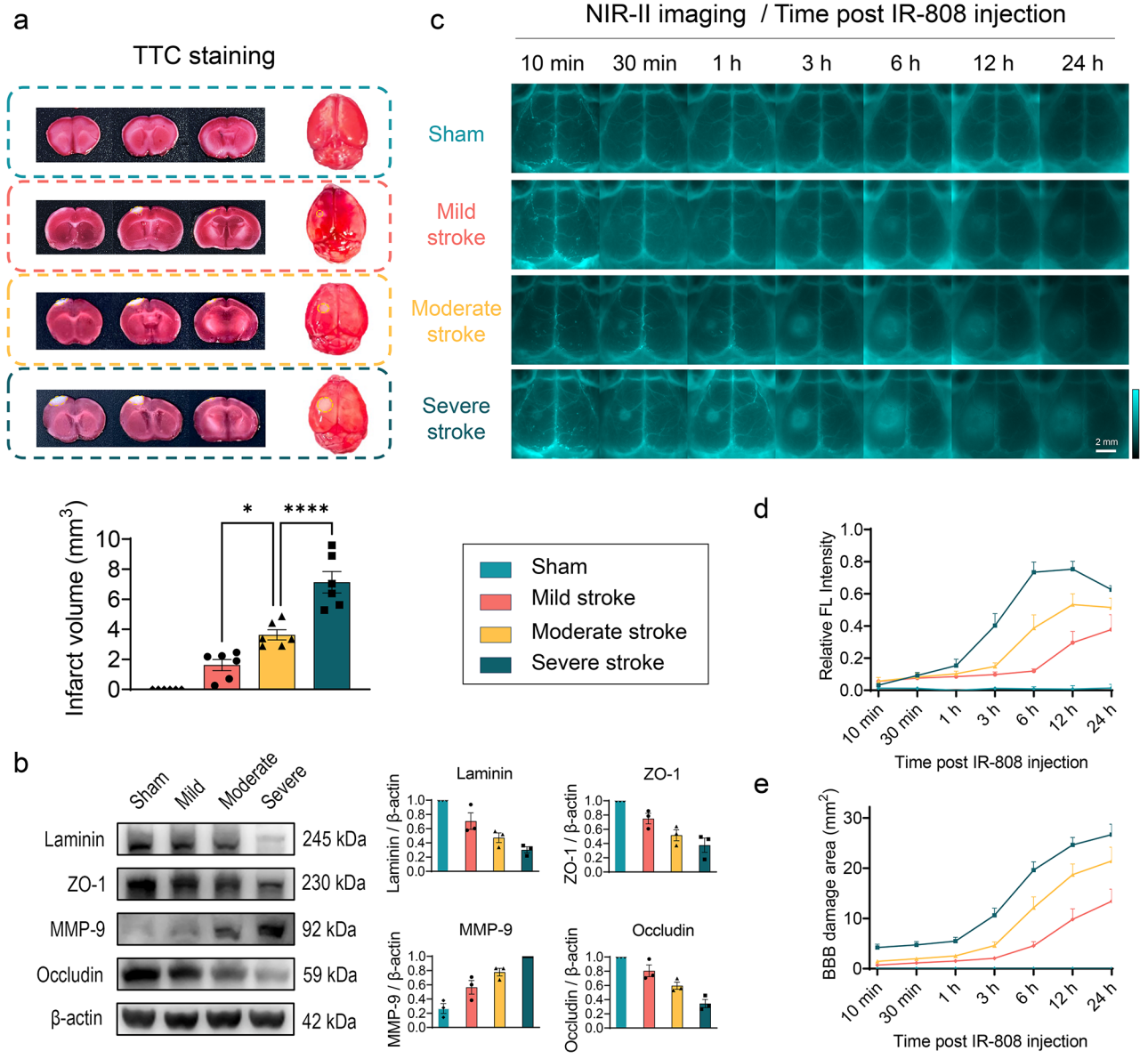

Fig. 4 IR-808 dynamic monitoring of BBB disruption with varying severity. (**a**) Coronal slices and whole-brain TTC staining in sham, mild, moderate, severe stroke groups and statistical analysis of infarct volumes quantified in slices (mean ± SEM, $n = 6$ for each group). (**b**) Western blotting analysis of BBB injury protein expression in the brains of mice with stroke with incremental severity (mean ± SEM, $n = 3$ for each group). (**c**) IR-808 NIR-II imaging for in vivo multi-timepoint monitoring of BBB disruption in strokes of different severity (40 ms, 1100 LP). (**d**) Quantification of the relative FL intensity (Ratio of fluorescence intensity of affected side/healthy side-1) at time post-injection ($n = 6$ for each group). (**e**) Quantification of the area of fluorescence signal accumulation in the BBB damage area at time post-injection ($n = 6$ for each group). *$P < 0.05$, ****$P < 0.0001$

well as EB leakage area and quantification were analyzed in the same mice (Fig. 5a).

Figure 5b present IR-808 in vivo and EB ex vivo imaging of mild, moderate, and severe strokes at 6 h, 12 h, and 24 h post-stroke. The relative fluorescence intensity of IR-808 correlated well with EB quantification at 6 h ($r = 0.975$, $P < 0.001$), 12 h ($r = 0.964$, $P < 0.001$), and 24 h ($r = 0.851$, $P < 0.001$) (Fig. 5c). This indicates that the quantitative evaluation of BBB injury by using IR-808 in vivo imaging is of high reliability. We further analyzed the findings in the brain sections (Fig. 5d). EB leakage and accumulation of IR-808 fluorescence signal can be quantified in sections (Figs. S10, S11). The fluorescence intensity quantification of IR-808 counted in sections correlated well with the relative fluorescence intensity in vivo (6 h: $r = 0.921$; 12 h: $r = 0.857$; 24 h: $r = 0.879$, all $P < 0.001$), demonstrating that in vivo NIR-II imaging has a good accuracy in reflecting IR-808 leakage into brain tissue (Fig. S12a). And the NIR fluorescence intensity in the sections correlated with EB quantification validating

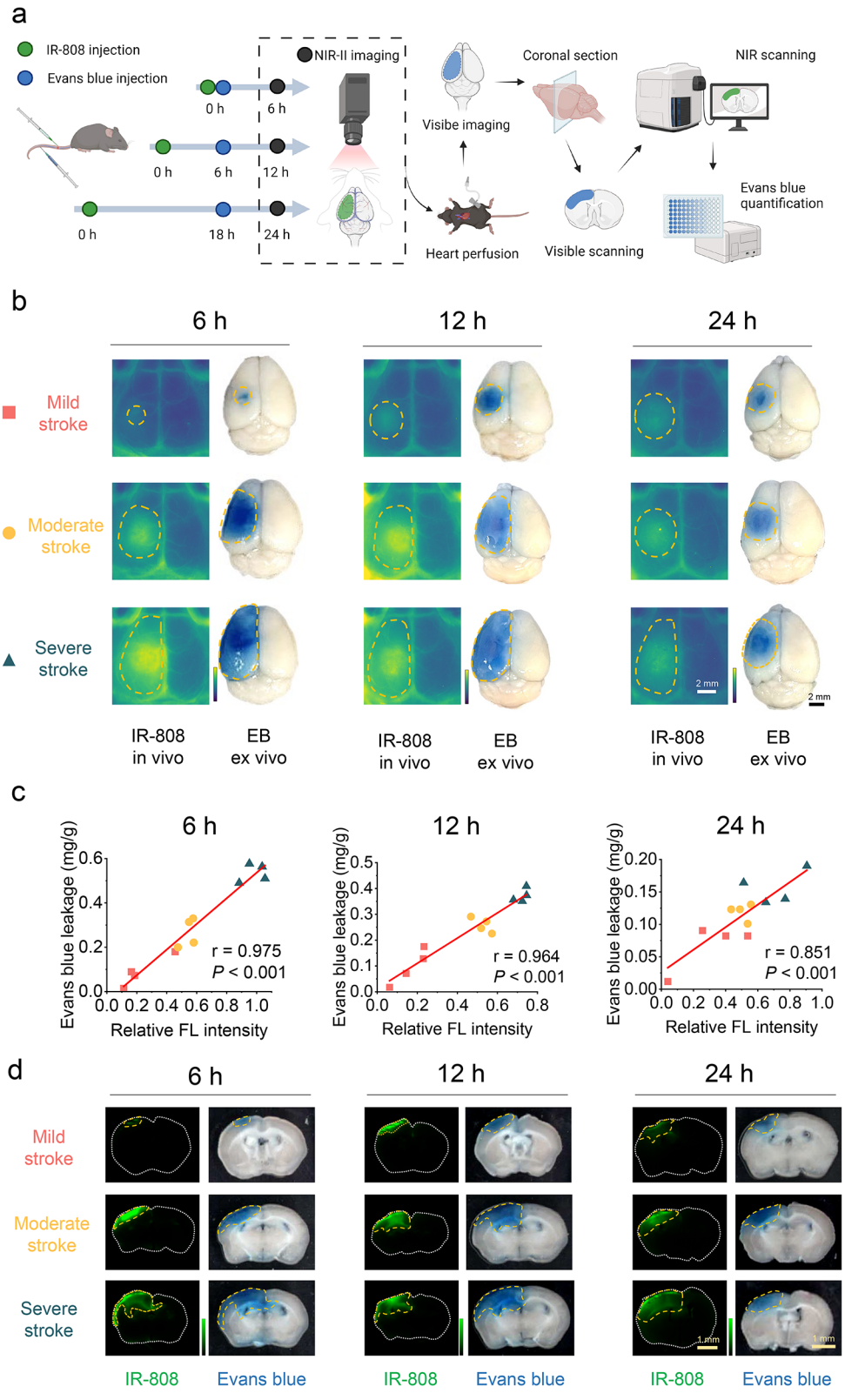

Fig. 5 Correlation of IR-808 with Evans blue evaluation of BBB injury. (**a**) Schematic diagram showing the quantification of IR-808 and Evans blue (EB) on BBB disruption evaluation in the same mice (Created with BioRender.com). (**b**) IR-808 in vivo NIR-II imaging and its ex vivo visible EB imaging in mice with mild, moderate, and severe stroke at 6 h, 12 h, and 24 h. Orange dotted line outlines BBB leakage areas. (**c**) Correlation of relative FL intensity of IR-808 with Evans blue quantification at 6 h, 12 h, and 24 h ($n = 12$ each time point). (**d**) The corresponding images of brain sections under NIR and visible scanning in panel b

the results of in vivo imaging (Fig. S12b). Furthermore, the size ratio of BBB disruption in whole brain measured by IR-808 to EB at 6 h, 12 h and 24 h was 1.045±0.039, 1.005±0.047, and 1.396±0.063, respectively, indicating that the IR-808 is reliable in assessing the area of leakage (Fig. S12c, d). Comparing multiple time points in vivo and ex vivo with EB, our results demonstrate the accuracy of IR-808 NIR-II imaging for repeat assessment of BBB injury in vivo.

In addition, to explore the correlation between BBB leakage assessed by IR-808 and final infarct volume, we also assessed the correlation at 6 h, 12 h and 24 h of dynamic monitoring in various severities stroke. The relative fluorescence intensity at 6 h (r=0.903, P<0.001), 12 h (r=0.825, P<0.001), and 24 h (r=0.659, P=0.003) as well as the area of BBB leakage at 6 h (r=0.880, P<0.001), 12 h (r=0.785, P<0.001), and 24 h (r=0.779, P<0.001), correlated with the final infarct volume (Fig. S13). These results suggest that monitoring BBB disruption by IR-808 allows for early prediction of the final infarct volume during dynamic monitoring.

Dual-channel NIR-II dynamic imaging simultaneously evaluates BBB injury and cerebral perfusion

Brain neuropathology changes complex after stroke, and changes in BBB damage often accompanied with dynamic changes in cerebral perfusion. Thus, dual-channel NIR-II imaging for simultaneous evaluation of BBB injury and cerebral perfusion has a high clinical applicability. IR-808 under 808 nm excitation showed the area of BBB disruption. To assess cerebral perfusion while monitoring the BBB, we employed another NIR-II probe, CO-1080@BSA, under 980 nm excitation and was intravenously injected at 6 h after stroke (Fig. 6a, b) [42]. Dynamic cerebrovascular images were captured beginning with injection of CO-1080@BSA. NIR-II images showed BBB leakage (808 nm, IR-808) and dynamic changes of the cerebrovascular arterial to venous phase (980 nm, CO-1080@BSA) in the two NIR-II imaging channels (Fig. 6c). We quantified the dynamic fluorescence signals of the cerebral blood vessels in the BBB leakage area and corresponding healthy side. Compared with that in the healthy side, the cerebral perfusion was significantly reduced in the BBB leakage area (Fig. 6d). We performed principal component analysis (PCA) on a series of 40-frame dynamic images to distinguish the arteries (red) and veins (blue) in the mouse brain vasculature and merged them with BBB leakage (green) (Fig. 6e). PCA revealed reduced arteries in the core of the ischemic area, while arterial vessels were still present in the surrounding BBB injury area. The real-time dual-channel NIR-II imaging system can observe changes in cerebral perfusion dynamics while evaluating BBB injury, which helps to insight the mechanism of neurological injury after stroke, and has good potential for in vivo and clinical application.

NIR-II BBB imaging provides real-time assessment of thrombolytic therapy efficacy and favorable biosafety

Thrombolytic therapy is a crucial reperfusion therapy in acute ischemic stroke, but reperfusion may aggravate BBB disruption [43, 44]. Therefore, it is necessary to evaluate the BBB and cerebrovascular perfusion in real time. We performed NIR-II BBB imaging in a mouse thrombolytic therapy model, achieving simultaneous dynamic assessment of cerebrovascular perfusion and BBB injury before and after thrombolysis (Fig. S14a). After stroke, middle cerebral artery (MCA) occlusion and reduced perfusion on the affected side were observed using IR-808 at 808 nm channel (Fig. S14b). After thrombolysis, MCA revascularization and perfusion recovery were observed at 980 nm channel using CO-1080@BSA (Fig. S14c). Meanwhile, BBB injury can be evaluated before and after thrombolysis in real-time, with the potential to guide treatment (Fig. S14d-f). To further verify the universality of our method, we successfully performed dynamic imaging of BBB disruption in a mouse permanent middle cerebral artery occlusion model (Fig. S15) and a rat PTS model (Fig. S16). These results demonstrate the potential wide applicability of albumin-seeking probe combined with NIR-II imaging for stroke BBB evaluation.

Considering its potential clinical applications, we tested complete metabolism in stroke brain tissue, effect on BBB recovery after stroke, and systemic safety. Fluorescence signals accumulating in stroke brain tissue were completely metabolized 2 weeks after IR-808 injection (Fig. S17a-b). At 14 d, the effects of the retention of IR-808 on brain tissue function were evaluated by behavioral tests and H&E staining. Behavioral tests results showed no significant difference in unilateral sensorimotor dysfunction and cognitive function between IR-808 group and PBS group (Fig. S17c). H&E staining showed the histopathological changes of peri-infarct tissue at 14 d after stroke was not significantly different between IR-808 group and PBS group (Fig. S17d). These results indicate that IR-808 retention did not impair brain tissue function. In addition, BBB leakage was measured by EB in stroke mice injected with IR-808 or PBS at 7 d, 14 d, and 21 d after stroke, respectively. The results showed no significant difference in EB leakage between the IR-808 and PBS groups, indicating that the use of IR-808 has no impact on BBB repair after stroke (Fig. S17e). In addition, serum from mice co-injected with IR-808 and CO-1080@BSA showed blood clearance under 808 nm and 980 nm excitation, respectively (Fig. S18a). Liver function, kidney function, and blood routine indices were within the normal range in mice treated with IR-808 or IR-808 plus CO-1080@BSA (Fig. S18b). H&E staining showed no

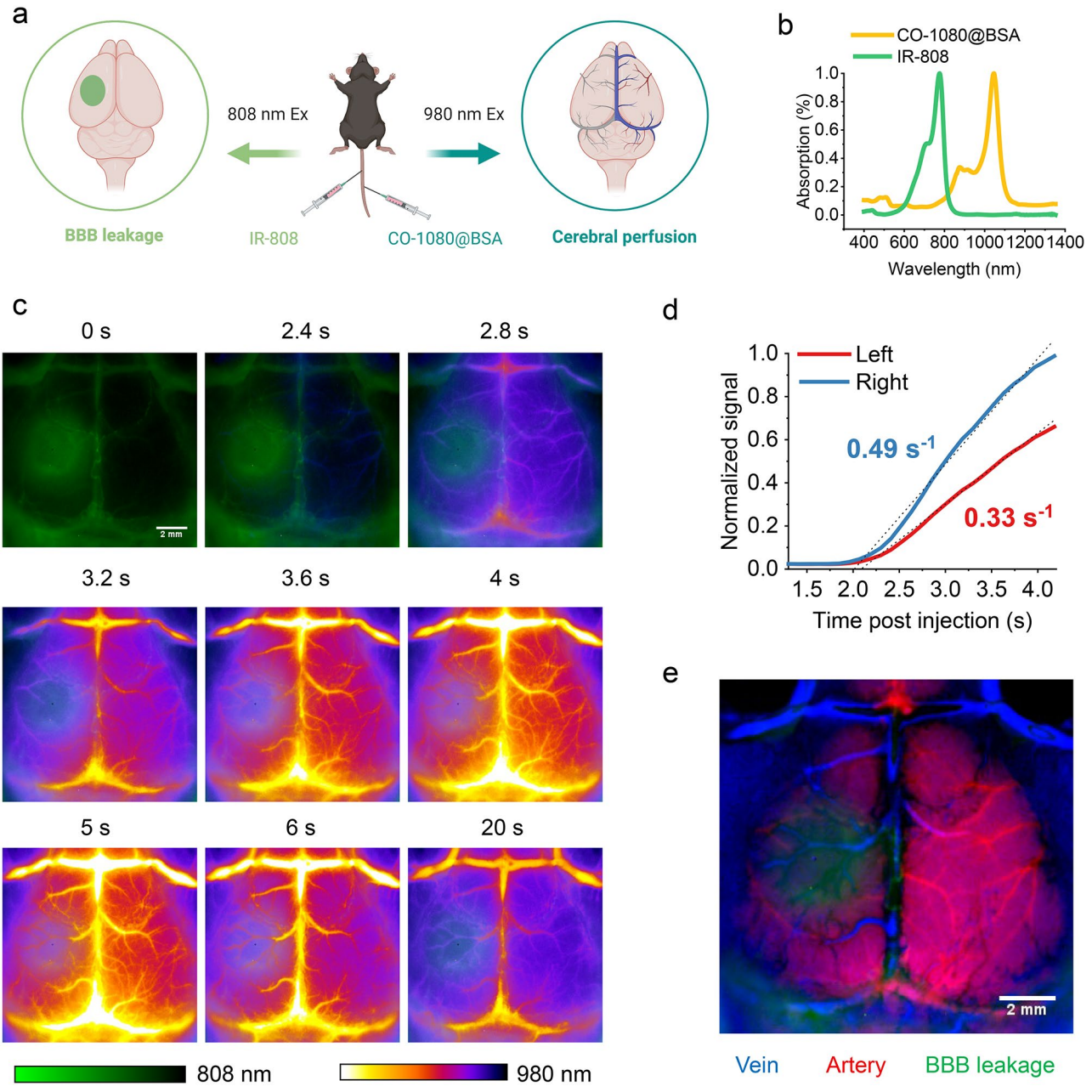

Fig. 6 Dual-channel NIR-II imaging of BBB disruption and cerebral perfusion after stroke. (**a**) Schematic diagram of dual-channel for BBB and cerebral perfusion imaging (Created with BioRender.com). (**b**) The absorption spectra of IR-808 and CO-1080@BSA. (**c**) Dual-channel images of the BBB and cerebral vascular (100 ms, 1200 LP) after stroke at time post CO-1080@BSA injection. IR-808 was used to evaluate BBB disruption using 808 nm laser excitation, while CO-1080@BSA was used to dynamically evaluate the cerebral vascular using 980 nm excitation at 6 h post stroke. (**d**) Fluorescence intensity (normalized to the right-side peak) versus time in the left (infarct side) and right (contralateral) sides of the brain of mice with stroke showed a significant reduction in perfusion in the stroke area. (**e**) Dynamic sequential images of vessels with CO-1080@BSA were analyzed by principal component analysis and merged with images of the BBB leakage area (green) to resolve arterial (red) and venous (blue) cerebral vessels

significant histological damage to the heart, liver, spleen, lungs, kidneys, or brain compared to the PBS group (Fig. S18c). These findings suggest that IR-808 and the co-injection of IR-808 plus CO-1080@BSA was safe and promising for clinical translation to in vivo NIR-II imaging of stroke.

Discussion

This study demonstrates that the albumin-seeking NIR probe binds to albumin in situ, allowing for high temporal and spatial resolution imaging of the location and extent of BBB dysfunction in vivo. This BBB imaging technique exhibits broad applicability and safety, enabling accurate quantitative analysis and serial monitoring of BBB injury.

Since albumin is virtually lacking in normal brain tissue and BBB disruption after stroke leads to albumin in the blood could cross the damaged BBB into brain tissue, the properties of albumin allow it to be used as a biomarker of BBB disruption after stroke [25, 26]. This pathophysiologic feature makes the albumin-seeking strategy to be a reliable method for evaluating BBB injury that the albumin-seek probes bind to albumin in the blood and enter the brain tissue with the tagged albumin to the BBB disruption area specifically. The results of in vitro and in vivo experiments demonstrated the effectiveness of albumin-seeking dyes bind to albumin highly selectively and stably in situ after intravenous injection, and covalent binding of IR-808 to albumin of 1:1 binding ratio allow quantification with accuracy as well as improving imaging properties [27]. IR-808@albumin fluorophores accumulate in brain tissue through disrupted BBB but not in the sham group. With the comparison of EB and TTC measurements, IR-808 accurately evaluated BBB injury of varying severity at multi-time points in a mouse stroke model. Our results provide an albumin-seeking strategy for real-time, accurate assessment of BBB injury in vivo.

BBB injury occurs ultra-early after stroke and progresses rapidly, therefore high temporal and spatial resolution and repeated evaluation capability are essential for BBB in vivo imaging. Most of the current experimental animal studies used EB staining, which limits the assessment in the same individual as well as in vivo. Several in vivo imaging methods are used in experimental animals but still have some limitations. Two-photon microscopy allows visualization of vascular leakage, but requires a cranial window and has a limited field of view [45]. MRI has low temporal resolution that makes it more challenging for repeated imaging [46]. CT has also been used to evaluate BBB injury after stroke but requires intra-arterial injection of contrast materials and remaining radiation exposure risk [47]. Several fluorescent probes have been reported that can be used to assess BBB damage after stroke (**Table S3**), but still lacking fluorescent probes that allow in vivo, high-resolution, real-time, non-invasive imaging. Advantageously, our NIR-II fluorescence imaging has low tissue autofluorescence and high SBR, with high spatial and temporal resolution for repetitive assessment of stroke in vivo [48]. NIR-II imaging combined with albumin-seeking probe allows for multi-time point and high-resolution visualization of BBB disruption in real time. In addition, we constructed a dual-channel NIR-II imaging to provide a visual imaging method for evaluating BBB and cerebral perfusion simultaneously and performed it in a mouse thrombolytic therapy model. This method provides timely assessment of reperfusion effects of thrombolytic therapy as well as real-time assessment of BBB injury progression before and after thrombolysis to guide therapy. Intravenous thrombolytic therapy is a crucial reperfusion treatment in the acute phase of stroke, but there is still a large portion of patients having poor prognosis [49], which mainly due to unsuccessful reperfusion and/or hemorrhagic transformation (caused by BBB injury after thrombolytic therapy) [50]. Real-time monitoring of reperfusion and BBB injury in stroke model is very important for the study of intravenous thrombolysis combined multiple treatment strategies. For example, the effect of the early application of antiplatelet drugs on vascular revascularization and its impact on the destruction of the BBB, the effect of new thrombolytic drugs and their influence on BBB, the protective effect of novel neuroprotective drugs on BBB after intravenous thrombolysis and so on. The study of these problems is very important for the formulation of comprehensive treatment strategies for patients with intravenous thrombolysis. In addition, our method allows for monitoring reperfusion and BBB injury in a real-time manner of thrombolytic therapy with pathological models of stroke combined with a variety of other diseases, such as hyperglycemic stroke model and hyperlipidemic stroke model, which can help to further understand the stroke pathogenesis mechanisms. In conclusion, our methods provide a broad prospect for non-invasive diagnosis of stroke and treatment efficacy assessment in clinical practice.

Furthermore, our work offers a biologically safe imaging strategy considering the possible risks of exogenous albumin. Encapsulation of cyanine dyes with albumin is an effective strategy to improve the brightness and pharmacokinetics for NIR-II bioimaging [27]. However, exogenous albumin carries the potential risk of contamination by blood-borne pathogens [51]. In addition, exogenous albumin is immunoreactive and may cause inflammation [37]. Minimizing the adverse effects is an important aspect of BBB monitoring to achieve clinical translation. Our study shows that IR-808 high selectively binds to endogenous albumin in situ and achieves the comparable effect as the dye-albumin complex that binds to BSA in vitro. This albumin-seeking dye exhibits good stability and biocompatibility, and is excreted in a timely manner post imaging with no impact on BBB recovery, which has great potential for clinical translation.

Conclusions

In summary, we demonstrate the albumin-seeking NIR probe allows for high-sensitivity and high-resolution imaging of the location and extent of BBB disruption in a safe, non-invasive and real-time manner. The albumin-seeking probe has a wide range of applications in BBB evaluation of stroke. Our NIR-II BBB imaging provides the potential for comprehensive evaluation of stroke pathophysiology, pathogenesis, and the development of effective therapeutic strategies.

Supplementary Information

The online version contains supplementary material available at https://doi.org/10.1186/s12951-024-02973-9.

Supplementary Material 1

Acknowledgements
The authors would like to acknowledge the researchers at Stroke Center of the First Hospital of Jilin University for providing helpful comments and discussion and sincerely thank all the members of the Joint Laboratory of Opto-Functional Theranostics in Medicine and Chemistry.

Author contributions
HJZ, SZ, YY and ZNG conceptualized and designed the study. HJZ and YYS performed the experiments and analyzed the data. The first draft of the manuscript was written by HJZ. YD and SZ helped revise the manuscript. SYZ, YQ, and SYP helped analyze the data. All authors read and approved the final manuscript.

Funding
This project was supported by the National Natural Science Foundation of China (823B2025) to YYS; the National Natural Science Foundation of China (82271303), the Talent Reserve Program of the First Hospital of Jilin University (JDYYCB-2023002) and Jilin University Young Teachers and Students Cross-disciplinary Cultivation Project (2024-JCXK-03) to ZNG; Norman Bethune Health Science Center of Jilin University (2022JBGS03), Science and Technology Department of Jilin Province (YDZJ202302CXJD061, 20220303002SF) and Jilin Provincial Key Laboratory (YDZJ202302CXJD017) to YY.

Data availability
No datasets were generated or analysed during the current study.

Declarations

Ethics approval and consent to participate
This study was approved by the Animal Ethical Committee of The First Hospital of Jilin University (20210642) and conforms to all the relevant guidelines and regulations.

Consent for publication
Not applicable.

Competing interests
The authors declare no competing interests.

Author details
[1]Stroke Center, Department of Neurology, The First Hospital of Jilin University, Chang Chun, China
[2]Neuroscience Research Center, Department of Neurology, The First Hospital of Jilin University, Chang Chun, China
[3]Joint Laboratory of Opto-Functional Theranostics in Medicine and Chemistry, The First Hospital of Jilin University, Changchun 130021, P.R. China
[4]State Key Laboratory of Supramolecular Structure and Materials, Center for Supramolecular Chemical Biology, College of Chemistry, Jilin University, Changchun 130012, P.R. China

Received: 17 July 2024 / Accepted: 3 November 2024
Published online: 29 November 2024

References

1. Global burden of. 288 causes of death and life expectancy decomposition in 204 countries and territories and 811 subnational locations, 1990–2021: a systematic analysis for the global burden of Disease Study 2021. Lancet. 2024;403(10440):2100–32.
2. Sweeney MD, Zhao Z, Montagne A, Nelson AR, Zlokovic BV. Blood-brain barrier: from physiology to Disease and back. Physiol Rev. 2019;99(1):21–78.
3. Liebner S, Dijkhuizen RM, Reiss Y, Plate KH, Agalliu D, Constantin G. Functional morphology of the blood-brain barrier in health and disease. Acta Neuropathol. 2018;135(3):311–36.
4. Ballabh P, Braun A, Nedergaard M. The blood-brain barrier: an overview: structure, regulation, and clinical implications. Neurobiol Dis. 2004;16(1):1–13.
5. Chen AQ, Fang Z, Chen XL, Yang S, Zhou YF, Mao L, et al. Microglia-derived TNF-α mediates endothelial necroptosis aggravating blood brain-barrier disruption after ischemic stroke. Cell Death Dis. 2019;10(7):487.
6. Bellut M, Papp L, Bieber M, Kraft P, Stoll G, Schuhmann MK. NLPR3 inflammasome inhibition alleviates hypoxic endothelial cell death in vitro and protects blood-brain barrier integrity in murine stroke. Cell Death Dis. 2021;13(1):20.
7. Jiang Q, Ewing JR, Ding GL, Zhang L, Zhang ZG, Li L, et al. Quantitative evaluation of BBB permeability after embolic stroke in rat using MRI. J Cereb Blood Flow Metab. 2005;25(5):583–92.
8. Bernardo-Castro S, Sousa JA, Brás A, Cecília C, Rodrigues B, Almendra L, et al. Pathophysiology of blood-brain barrier permeability throughout the different stages of ischemic stroke and its implication on Hemorrhagic Transformation and Recovery. Front Neurol. 2020;11:594672.
9. Knowland D, Arac A, Sekiguchi KJ, Hsu M, Lutz SE, Perrino J, et al. Stepwise recruitment of transcellular and paracellular pathways underlies blood-brain barrier breakdown in stroke. Neuron. 2014;82(3):603–17.
10. Harris WJ, Asselin MC, Hinz R, Parkes LM, Allan S, Schiessl I, et al. In vivo methods for imaging blood-brain barrier function and dysfunction. Eur J Nucl Med Mol Imaging. 2023;50(4):1051–83.
11. Wu X, Li JR, Fu Y, Chen DY, Nie H, Tang ZP. From static to dynamic: live observation of the support system after ischemic stroke by two photon-excited fluorescence laser-scanning microscopy. Neural Regen Res. 2023;18(10):2093–107.
12. Vahrmeijer AL, Hutteman M, van der Vorst JR, van de Velde CJ, Frangioni JV. Image-guided cancer surgery using near-infrared fluorescence. Nat Rev Clin Oncol. 2013;10(9):507–18.
13. Tian R, Zeng Q, Zhu S, Lau J, Chandra S, Ertsey R, et al. Albumin-chaperoned cyanine dye yields superbright NIR-II fluorophore with enhanced pharmacokinetics. Sci Adv. 2019;5(9):eaaw0672.
14. Xu J, Du Y, Han T, Zhu N, Zhu S. Protein@Cyanine-Based NIR-II Lymphography enables the Supersensitive Visualization of Lymphedema and Tumor Lymphatic Metastasis. Adv Healthc Mater. 2023:e2301051.
15. Hong G, Lee JC, Robinson JT, Raaz U, Xie L, Huang NF, et al. Multifunctional in vivo vascular imaging using near-infrared II fluorescence. Nat Med. 2012;18(12):1841–6.
16. Antaris AL, Chen H, Diao S, Ma Z, Zhang Z, Zhu S, et al. A high quantum yield molecule-protein complex fluorophore for near-infrared II imaging. Nat Commun. 2017;8:15269.
17. Antaris AL, Chen H, Cheng K, Sun Y, Hong G, Qu C, et al. A small-molecule dye for NIR-II imaging. Nat Mater. 2016;15(2):235–42.
18. Zhang X, Li S, Ma H, Wang H, Zhang R, Zhang XD. Activatable NIR-II organic fluorescent probes for bioimaging. Theranostics. 2022;12(7):3345–71.
19. Yang L, Gao Y, Wei J, Cheng Z, Wu S, Zou L, et al. Selenium-integrated conjugated oligomer nanoparticles with high photothermal conversion efficiency for NIR-II imaging-guided cancer phototheranostics in vivo. J Nanobiotechnol. 2023;21(1):314.
20. Fan Y, Wang P, Lu Y, Wang R, Zhou L, Zheng X, et al. Lifetime-engineered NIR-II nanoparticles unlock multiplexed in vivo imaging. Nat Nanotechnol. 2018;13(10):941–6.
21. Yang RQ, Lou KL, Wang PY, Gao YY, Zhang YQ, Chen M, et al. Surgical Navigation for malignancies guided by Near-Infrared-II fluorescence imaging. Small Methods. 2021;5(3):e2001066.
22. Wang Z, Wang X, Wan JB, Xu F, Zhao N, Chen M. Optical imaging in the Second Near Infrared Window for Vascular Bioimaging. Small. 2021;17(43):e2103780.
23. Zhang K, Chen FR, Wang L, Hu J. Second Near-Infrared (NIR-II) window for imaging-navigated modulation of Brain structure and function. Small. 2023;19(14):e2206044.
24. Huang D, Wang Q, Cao Y, Yang H, Li M, Wu F, et al. Multiscale NIR-II imaging-guided brain-targeted drug delivery using Engineered Cell membrane Nanoformulation for Alzheimer's Disease Therapy. ACS Nano. 2023;17(5):5033–46.
25. Tamaki K, Sadoshima S, Heistad DD. Increased susceptibility to osmotic disruption of the blood-brain barrier in chronic hypertension. Hypertension. 1984;6(5):633–8.

26. Fujihara R, Chiba Y, Nakagawa T, Nishi N, Murakami R, Matsumoto K, et al. Albumin microvascular leakage in brains with diabetes mellitus. Microsc Res Tech. 2016;79(9):833–7.
27. Bai L, Hu Z, Han T, Wang Y, Xu J, Jiang G, et al. Super-stable cyanine@albumin fluorophore for enhanced NIR-II bioimaging. Theranostics. 2022;12(10):4536–47.
28. Xu J, Zhu N, Du Y, Han T, Zheng X, Li J, et al. Biomimetic NIR-II fluorescent proteins created from chemogenic protein-seeking dyes for multicolor deep-tissue bioimaging. Nat Commun. 2024;15(1):2845.
29. Tian R, Feng X, Wei L, Dai D, Ma Y, Pan H, et al. A genetic engineering strategy for editing near-infrared-II fluorophores. Nat Commun. 2022;13(1):2853.
30. Capistrano G, Sousa-Junior AA, Silva RA, Mello-Andrade F, Cintra ER, Santos S, et al. IR-780-albumin-based Nanocarriers promote Tumor Regression not only from Phototherapy but also by a nonirradiation mechanism. ACS Biomater Sci Eng. 2020;6(8):4523–38.
31. Usama SM, Park GK, Nomura S, Baek Y, Choi HS, Burgess K. Role of Albumin in Accumulation and Persistence of Tumor-seeking cyanine dyes. Bioconjug Chem. 2020;31(2):248–59.
32. Vita GM, De Simone G, De Marinis E, Nervi C, Ascenzi P, di Masi A. Serum albumin and nucleic acids biodistribution: from molecular aspects to biotechnological applications. IUBMB Life. 2022;74(9):866–79.
33. Takeuchi T, Kitayama Y, Sasao R, Yamada T, Toh K, Matsumoto Y, et al. Molecularly imprinted nanogels acquire Stealth in situ by cloaking themselves with native Dysopsonic proteins. Angew Chem Int Ed Engl. 2017;56(25):7088–92.
34. Kuang Y, Zhang K, Cao Y, Chen X, Wang K, Liu M, et al. Hydrophobic IR-780 dye encapsulated in cRGD-Conjugated solid lipid nanoparticles for NIR Imaging-guided Photothermal Therapy. ACS Appl Mater Interfaces. 2017;9(14):12217–26.
35. Calvo CF, Amigou E, Tencé M, Yoshimura T, Glowinski J. Albumin stimulates monocyte chemotactic protein-1 expression in rat embryonic mixed brain cells. J Neurosci Res. 2005;80(5):707–14.
36. Klohs J, Steinbrink J, Bourayou R, Mueller S, Cordell R, Licha K, et al. Near-infrared fluorescence imaging with fluorescently labeled albumin: a novel method for non-invasive optical imaging of blood-brain barrier impairment after focal cerebral ischemia in mice. J Neurosci Methods. 2009;180(1):126–32.
37. Chruszcz M, Mikolajczak K, Mank N, Majorek KA, Porebski PJ, Minor W. Serum albumins-unusual allergens. Biochim Biophys Acta. 2013;1830(12):5375–81.
38. Jiang C, Cheng H, Yuan A, Tang X, Wu J, Hu Y. Hydrophobic IR780 encapsulated in biodegradable human serum albumin nanoparticles for photothermal and photodynamic therapy. Acta Biomater. 2015;14:61–9.
39. Du Y, Xu J, Zheng X, Dang Z, Zhu N, Jiang Z et al. NIR-II protein-escaping dyes enable high-contrast and long-term prognosis evaluation of flap transplantation. Adv Mater. 2023:e2311515.
40. Uzdensky AB. Photothrombotic Stroke as a model of ischemic stroke. Transl Stroke Res. 2018;9(5):437–51.
41. Saunders NR, Dziegielewska KM, Møllgård K, Habgood MD. Markers for blood-brain barrier integrity: how appropriate is Evans blue in the twenty-first century and what are the alternatives? Front Neurosci. 2015;9:385.
42. Zhang Y, Jia Y, Zhu S. NIR-II cyanine@albumin fluorophore for deep tissue imaging and imaging-guided surgery. SmartMat. 2024;5(4):e1245.
43. Tsivgoulis G, Katsanos AH, Sandset EC, Turc G, Nguyen TN, Bivard A, et al. Thrombolysis for acute ischaemic stroke: current status and future perspectives. Lancet Neurol. 2023;22(5):418–29.
44. Yang N, Lee H, Wu C. Intravenous thrombolysis for acute ischemic stroke: from alteplase to tenecteplase. Brain Circ. 2023;9(2):61–3.
45. Underly RG, Levy M, Hartmann DA, Grant RI, Watson AN, Shih AY. Pericytes as inducers of Rapid, Matrix Metalloproteinase-9-Dependent Capillary damage during ischemia. J Neurosci. 2017;37(1):129–40.
46. Vlachos F, Tung YS, Konofagou EE. Permeability assessment of the focused ultrasound-induced blood-brain barrier opening using dynamic contrast-enhanced MRI. Phys Med Biol. 2010;55(18):5451–66.
47. Park JY, Lee SK, Kim JY, Je KH, Schellingerhout D, Kim DE. A new micro-computed tomography-based high-resolution blood-brain barrier imaging technique to study ischemic stroke. Stroke. 2014;45(8):2480–4.
48. Chen Y, Yang Y, Zhang F. Noninvasive in vivo microscopy of single neutrophils in the mouse brain via NIR-II fluorescent nanomaterials. Nat Protoc. 2024;19(8):2386–407.
49. Hacke W, Kaste M, Bluhmki E, Brozman M, Dávalos A, Guidetti D, et al. Thrombolysis with alteplase 3 to 4.5 hours after acute ischemic stroke. N Engl J Med. 2008;359(13):1317–29.
50. van Kranendonk KR, Treurniet KM, Boers AMM, Berkhemer OA, van den Berg LA, Chalos V, et al. Hemorrhagic transformation is associated with poor functional outcome in patients with acute ischemic stroke due to a large vessel occlusion. J Neurointerv Surg. 2019;11(5):464–8.
51. Fanali G, di Masi A, Trezza V, Marino M, Fasano M, Ascenzi P. Human serum albumin: from bench to bedside. Mol Aspects Med. 2012;33(3):209–90.

Publisher's note